



# Material Characterization of MR Fluid on Performance of MRF Based Brake

Nguyen Vien Quoc<sup>1</sup>, Le Duy Tuan<sup>1</sup>, Le Dai Hiep<sup>2</sup>, Hung Nguyen Quoc<sup>2\*</sup> and Seung Bok Choi<sup>3\*</sup>

<sup>1</sup> Industrial University of Ho Chi Minh City, Ho Chi Minh City, Vietnam, <sup>2</sup> Faculty of Engineering, Vietnamese-German University, Binh Duong, Vietnam, <sup>3</sup> Department of Mechanical Engineering, Inha University, Incheon, South Korea

This study focuses on material characterizations of Magneto-rheological fluid (MRF) on performance characteristics of magneto-rheological brake (MRB). In this study, three different types of MRF (low viscosity, medium viscosity, and high viscosity) are considered for several types of MRB. Firstly, the optimization solution of the MRB design is proposed based on the Bingham plastic model of the MRFs and finite element analysis of MRB magnetic circuit. From optimal design of the MRBs with different MRFs, performance characteristics of the MRBs such as braking torque, off-state torque, and power consumption are evaluated. In addition, the compact size of MRB using different MRFs is also studied. Finally, some observations and guidance on selection of MRFs in MRB design are summarized.

**Keywords:** magneto-rheological fluid (MRF), conventional MR brake, material characterization, optimal design, side-coil MR brake

## OPEN ACCESS

### Edited by:

Weijia Wen,  
Hong Kong University of Science and  
Technology, Hong Kong

### Reviewed by:

Xiaomin Dong,  
Chongqing University, China  
Xufeng Dong,  
Dalian University of Technology (DUT),  
China

### \*Correspondence:

Hung Nguyen Quoc  
hung.nq@vgu.edu.vn  
Seung Bok Choi  
seungbok@inha.ac.kr

### Specialty section:

This article was submitted to  
Smart Materials,  
a section of the journal  
Frontiers in Materials

**Received:** 01 November 2018

**Accepted:** 14 May 2019

**Published:** 12 June 2019

### Citation:

Quoc NV, Tuan LD, Hiep LD, Quoc HN  
and Choi SB (2019) Material  
Characterization of MR Fluid on  
Performance of MRF Based Brake.  
Front. Mater. 6:125.  
doi: 10.3389/fmats.2019.00125

## INTRODUCTION

In last two decades, researches on the development and application of brake featuring magneto-rheological fluid (MRF) have interested many researchers. There have been numerous researches on improving performance of MRF based brake (MRB) with different configurations and applications such as: disc-type MRB (An and Kwon, 2003; Liu et al., 2006; Park et al., 2006), drum-type MRBs (Huang et al., 2002; Smith et al., 2007), hybrid-type MRB with T-shaped rotor (Avraam et al., 2008; Nguyen and Choi, 2012; Mousavi and Sayyaadi, 2018). Avraam et al performed some analyses and comparisons of different types of MRB such as disc-type, drum type, and T-shape type in development of a rotational MRB for rehabilitation devices (Avraam et al., 2010). Inmaduddin et al. reviewed advances in MRBs, in terms of various innovations of structural and magnetic circuit designs, including disc-type, drum-type, and hybrid type as well as modeling techniques that have been involved with each innovation (Imaduddin et al., 2013). In order to have a more detailed comparison of different types of MRB, Nguyen and Choi (2011) investigated the optimal design of different types of MRB considering their maximum braking torque and specific volume. Later, Nguyen et al. (2014a) evaluated the effect of different shapes of envelope such as the rectangular, the polygonal and the spline to the performance and the mass of MRBs. Recently, Nguyen et al. (2014b, 2015) proposed a new configuration of MRB in which a magnetic coil is wound on each side of the housing of the MRB (in this research, it is named as side-coil MRB). The results showed that, with this configuration, some disadvantages of the traditional MRBs such as the “bottle-neck” problem of magnetic flux, the non-magnetic bobbin requirement, difficulties in manufacturing and maintenance can be eliminated or minimized. In addition, the optimal solutions showed that the mass of the side-coil MRB was significantly improved in producing the same braking torque as the conventional ones.

In the design of MRB, different types of MRF have been used. However, how the characterization of MRF's effects on the performance of MRB was not considered in detail. In order to fill this gap, this research investigates the effects of MRF characterizations on the performance of MRB through simulation results, from which guidelines on the selection of MRF types for MRBs are summarized. The remainder of the paper is arranged as follows. In section Conventional and Side-Coil MRBs, several configurations of MRB considered in this study are introduced. After that, in section Optimization of MRBs Based on Finite Element Analysis, the optimization solution of the MRB design is proposed based on the Bingham plastic model of the MRFs and finite element analysis of MRB magnetic circuit. In section Results and Discussions, optimal solutions of the MRBs with different MRFs are obtained, from which, performance characteristics of the MRBs such as braking torque, off-state torque, and power consumption are evaluated. Finally, some observations and guidance on selection of MRFs in MRB design are summarized.

### CONVENTIONAL AND SIDE-COIL MRBS

As mentioned above, several types of MRB have been developed so far. In this study, two of the most typical types of MRB, the conventional disc-type MRB and the side-coil MRB, are considered. **Figure 1A** shows a typical conventional MRB and **Figure 1B** presents the side-coil one.

The first configuration represents conventional MRBs which use outside cylindrical coils such as disc-type, drum-type, while the second configuration represent for the MRBs which use side coils including T-shape MRBs. As shown in the figure, a disc (rotor) made of magnetic steel is fastened to the flange of the MRB shaft made of non-magnetic steel. The disc is embedded inside a stationary envelope (housing) made of magnetic steel. In **Figure 1A**, a wire-coil is wound on a non-magnetic bobbin which is fixed to the brake envelop while in **Figure 1B**, the coil is placed on each side housing of the brake. By using the side-coil configuration, it is observed that the coils can be placed directly on the housing. In addition, multiple coils can be implemented, especially for high braking torque MRBs.

It is obviously observed that the braking torque of the proposed MR brake comes from two sources: the friction of MRF acting on the two end-faces and on the outer annular face of the disc. Firstly, the friction between MRF and the end-faces of the disc is analyzed. The induced torque from MRF in radial duct acting on one end-face of a disc can be expressed as follows (Nguyen and Choi, 2012):

$$T_e = \int_A \tau_e r dA = 2\pi \int_{R_1}^{R_2} \tau_e r^2 dr \tag{1}$$

where  $A$  is the area of the end-face of the disc,  $r$  is the radius of an infinitesimal area of the disc,  $R_1$  and  $R_2$  are the inner and outer radius of the duct.  $\tau_e$  is the shear stress of the MRF at the interface, which can be predicted from the Bingham-plastic model of the MRF as follows:

$$\tau_e = \tau_{ye} + \mu_e \dot{\gamma}_e \tag{2}$$

where,  $\tau_{ye}$  and  $\mu_e$  are, respectively, the yield stress and post yield viscosity of the MRF.  $\dot{\gamma}_e$  is the shear rate of MR fluid at the interface. Because the gap size of the duct is very small, the shear rate of MRF in the gap is assumed to be linearly distributed which can be approximately determined as follows:

$$\dot{\gamma}_e = \frac{r\Omega}{d} \tag{3}$$

where  $d$  is the gap size and  $\Omega$  is the angular velocity of the drum.

Plug Equations (2, 3) into Equation (1) the following equation can be obtained.

$$T_e = 2\pi \int_{R_1}^{R_2} r^2 \mu_e \left( \frac{r\Omega}{d} \right) dr + 2\pi \int_{R_1}^{R_2} r^2 \tau_{ye} dr \tag{4}$$

Generally, the magnetic density in the MRF gap is a function of radius  $r$ , thus the values of  $\tau_{ye}$  and  $\mu_e$  of the MRF in the gap are also functions of  $r$ . Equation (4) then have to be calculated by numerically integrating. In order to facilitate the calculation, it is assumed that the magnetic density in the MRF gap is constant and an average value of the magnetic density obtained from numerical integration is used. In this case, Equation (4) can be analytically integrated to yield

$$T_e = \frac{\pi \mu_e R_2^4}{2d} \left[ 1 - \left( \frac{R_1}{R_2} \right)^4 \right] \Omega + \frac{2\pi \tau_{ye}}{3} (R_2^3 - R_1^3) \tag{5}$$

The torque due to MRF in annular gap acting on the outer circular face of the disc can be determined by

$$T_a = \int_{A_a} R_a \tau_a dA = \int_0^{L_a} R_a \tau_a 2\pi R_a dl = 2\pi R_a^2 \int_0^{L_a} (\tau_{ya} + \mu_a \dot{\gamma}) dl \tag{6}$$

where  $A_a$  is the area of the outer annular face of the disc,  $L_a$  and  $R_a$  are radius and length of annular duct,  $\tau_a$  is the shear stress at the annular face of the disc,  $\tau_{ya}$  and  $\mu_a$  are the yield stress and post yield viscosity of the MRF in the annular duct. Similarly to MRF in the end-face gap, by using average magnetic density obtained from numerical integration and assuming a linear distribution of shear rate in the MRF gap, the following can be obtained

$$T_a = 2\pi R_a^2 L_a \left( \tau_{ya} + \mu_a \frac{R_a \Omega}{d} \right) \tag{7}$$

From Equations (5) to (7), by neglecting friction torque from sealing and bearing, the induced braking torque of the

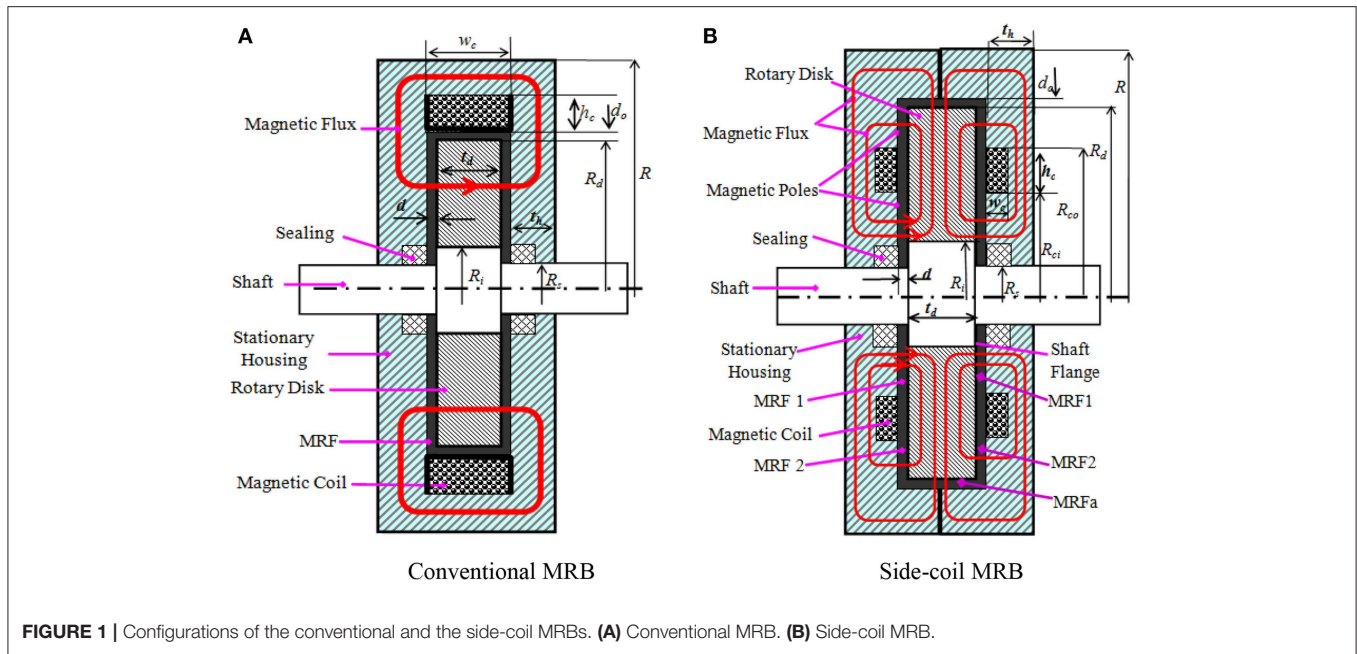


**FIGURE 1 |** Configurations of the conventional and the side-coil MRBs. **(A)** Conventional MRB. **(B)** Side-coil MRB.

conventional disc-type MRB and the side-coil ones can be correspondingly obtained

$$T_c = 2T_e + T_a = \frac{\pi \mu_e R_d^4}{d} \left[ 1 - \left( \frac{R_i}{R_d} \right)^4 \right] \Omega + \frac{4\pi \tau_{ye}}{3} (R_d^3 - R_i^3) + 2\pi R_d^2 t_d \left( \tau_{y0} + \mu_0 \frac{\Omega R_d}{d_o} \right) \quad (8)$$

$$T_s = 2(T_{e1} + T_{e2}) + T_a = \frac{\pi \mu_1 R_{ci}^4}{d} \left[ 1 - \left( \frac{R_i}{R_{ci}} \right)^4 \right] \Omega + \frac{4\pi \tau_{y1}}{3} (R_{ci}^3 - R_i^3) + \frac{\pi \mu_2 R_d^4}{d} \left[ 1 - \left( \frac{R_{co}}{R_d} \right)^4 \right] \Omega + \frac{4\pi \tau_{y2}}{3} (R_d^3 - R_{co}^3) + 2\pi R_d^2 t_d \left( \tau_{ya} + \mu_a \frac{\Omega R_d}{d_o} \right) \quad (9)$$

and the off-state force (the torque of the MRB when no magnetic field is applied to MRF) of both considered MRBs can be expressed as Nguyen et al. (2015).

$$T_0 = \frac{\pi \mu_0 R_d^4}{d} \left[ 1 - \left( \frac{R_s}{R_d} \right)^4 \right] \Omega + \frac{4\pi \tau_{y0}}{3} (R_d^3 - R_s^3) + 2\pi R_d^2 t_d \left( \tau_{y0} + \mu_0 \frac{\Omega R_d}{d_o} \right) + 2T_{sf} \quad (10)$$

where  $T_c$  is the braking torque of the conventional MRB,  $T_s$  is the braking torque of the side coil MRB,  $T_0$  is the off-state torque of MRBs,  $T_{e1}$  and  $T_{e2}$  are the friction torque of MRF in region 1 (MRF1) and MRF in region 2 (MRF2) acting on the disc in case of the side coil MRB,  $R_d$  is the outer radius of the disc,  $R_i$  is the inner radius of the active MRF volume in the end-face duct,  $R_s$  is the shaft diameter,  $d$  is the gap size of the end-face MRF ducts between the disc and the housing,  $d_o$  is the gap size of the annular MRF duct at the outer cylindrical face of the disc,  $t_d$  is the thickness of the disc,  $R_{ci}$  and  $R_{co}$  are the inner and outer

radii of the coil in the case of the side-coil MRB,  $\Omega$  is the angular velocity of the rotor,  $\mu_e$  and  $\tau_{ye}$  are, respectively, the average post yield viscosity and yield stress of MRF in the end-face duct of the conventional MRB,  $\mu_j$  is the average post yield viscosity of the  $j^{th}$  active MRF volume (denoted by MRF $j$ ) in the end-face duct of the side-coil MRBs while  $\tau_{yj}$  is the corresponding yield stress,  $\mu_a$  and  $\tau_{ya}$  are, respectively, the average post yield viscosity and yield stress of MRF in the annular duct of the side-coil MRBs,  $\tau_{y0}$  and  $\mu_0$  are the zero-field yield stress and viscosity of the MRF. The rheological properties of MRF such as the induced yield stress  $\tau_{ye}$ ,  $\tau_{yj}$ ,  $\tau_{ya}$ , and the corresponding average post yield viscosity  $\mu_e$ ,  $\mu_j$ ,  $\mu_a$  depend on the exerted magnetic flux density across the active MRF volumes and can be approximated by Zubieta et al. (2009).

$$Y = Y_\infty + (Y_0 - Y_\infty)(2e^{-B\alpha_{SY}} - e^{-2B\alpha_{SY}}) \quad (11)$$

where  $Y$  represents for a rheological parameters of MRF such as the yield stress and the post yield viscosity,  $Y_0$  and  $Y_\infty$ , respectively, represents for the value of  $Y$  in the absence of magnetic field and in saturated state of MRF,  $\alpha_{SY}$  is the saturation moment index of the  $Y$  parameter,  $B$  is the applied magnetic density.

## OPTIMIZATION OF MRBS BASED ON FINITE ELEMENT ANALYSIS

In this part, the optimal design problem of the conventional and the side-coil MRBs is constructed. In the design of MRBs, a required braking torque is usually given depending on the application. Therefore, the purpose of the MRB design is to determine geometric dimensions of the brake so that the brake can create a required braking torque while the mass of the brake

is as small as possible. In addition, the power consumption of the coils and the off-state torque are also important issues should be accounted for. The power consumption should be as small as possible to save energy and to accommodate with available power for each application. The off-state torque should be small to reduce the energy lost and also to reduce the heating problem. In this study, an objective function, which is a linear combination of the above issues, is proposed, which is mathematically expressed as the following:

$$Obj = \alpha_m \frac{m_b}{m_{ref}} + \alpha_p \frac{P}{P_{ref}} + \alpha_{T_0} \frac{T_0}{T_{0ref}} \quad (12)$$

In the above,  $m_b$ ,  $P$ , and  $T_0$  are, respectively, the mass, the power consumption and the off-state torque of the brake,  $m_{ref}$ ,  $P_{ref}$ , and  $T_{0ref}$  are, respectively, the reference mass, the power consumption and the off-state torque, and  $\alpha_m$ ,  $\alpha_p$ , and  $\alpha_{T_0}$  are the corresponding weighting coefficients determined based on the importance of the objectives. In this research, the reference values are obtained from the optimization problem in which the objective function is the mass of the MRB, Nguyen et al. (2014a, 2015). Generally, the MRB mass can be approximately calculated by Nguyen et al. (2015).

$$m_b = V_d \rho_d + V_h \rho_h + V_s \rho_s + V_{MR} \rho_{MR} + V_{bob} \rho_{bob} + V_c \rho_c \quad (13)$$

where  $V_d$ ,  $V_h$ ,  $V_s$ ,  $V_{MR}$ ,  $V_{bob}$ , and  $V_c$  are, respectively, the geometric volume of the disc, the housing, the shaft, the MRF, the bobbin and the coil of the brake,  $\rho_d$ ,  $\rho_h$ ,  $\rho_s$ ,  $\rho_{MR}$ ,  $\rho_{bob}$ , and  $\rho_c$  are correspondingly density of the discs, the housing, the shaft, the MRF, the bobbin in case of conventional MRB (in case of the side-coil MRBs, this term is eliminated) and the coil material.

Power consumption of the MRBs can be calculated by

$$P = I^2 R_w \quad (14)$$

where  $I$  is the electric current applied to the coils and  $R_w$  is the resistance of the coil wires, which can be approximately calculated as follows:

$$R_w = L_w r_w = 2\pi R_c N_c \frac{r}{A_w} = 2\pi R_c \varepsilon \frac{A_c}{A_w} \frac{r}{A_w} = \frac{2R_c \varepsilon w_c h_c r}{\pi d_w^2} \quad (15)$$

$$R_w = 2L_w r_w = 4\pi R_c N_c \frac{r}{A_w} = 4\pi R_c \varepsilon \frac{A_c}{A_w} \frac{r}{A_w} = \frac{4R_c \varepsilon w_c h_c r}{\pi d_w^2} \quad (16)$$

In the above,  $L_w$  is the length of the coil wire,  $r_w$  is the resistance per unit length of the coil wire,  $N_c$  is the number of coil turns,  $R_c$  is the average radius of the coil cross-sectional area,  $A_w$  is the cross sectional area of the wire,  $A_c$  is the cross sectional area of the coil,  $\varepsilon$  is the filling ratio of the coil which is assumed to be 0.8 in this study,  $r$  is the resistivity of the coil wire,  $r = 0.01726 \text{ } (\Omega\text{m})$  for copper wire.

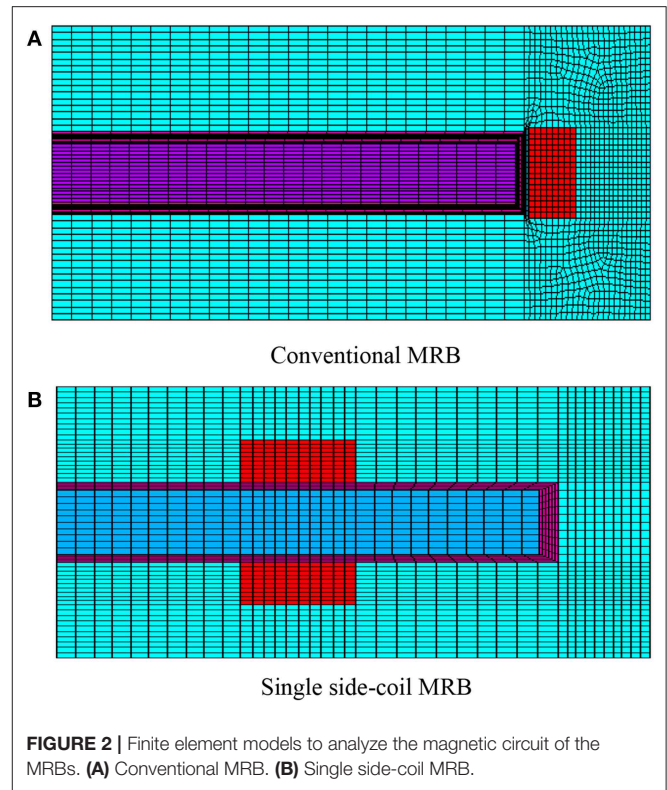
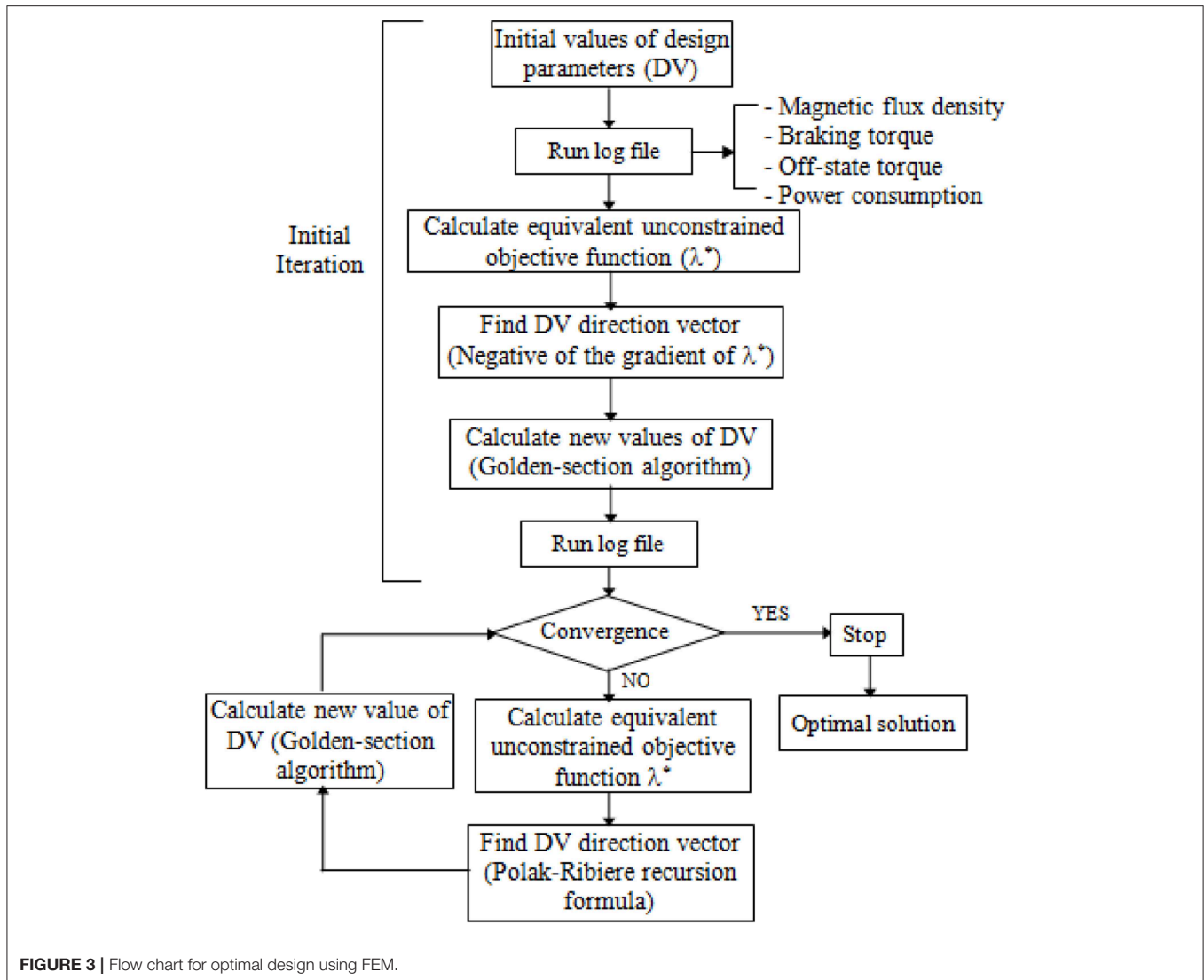


**FIGURE 2** | Finite element models to analyze the magnetic circuit of the MRBs. **(A)** Conventional MRB. **(B)** Single side-coil MRB.

In order to determine the braking torque of the MRBs, firstly, finite element analysis (FEA) is used to evaluate the magnetic density across the ducts of MRF based on quasi-static analysis. This is reasonable because the purpose of this research is to investigate the effect of MRF on performance characteristics of MRB and this can be archived by quasi-static simulation. In detail, the finite element models generated by 2D-axisymmetric couple element (PLANE 13) of commercial ANSYS software, as shown in **Figure 2**, are applied to solve the magnetic circuits of the MRB. It is noted in **Figure 2** that the mesh size is specified by the number of elements per line rather than element size and the number of elements on the lines across the MR duct is specified as a parameter called the basic meshing number. The number of elements of other lines is chosen as a product of the basic meshing number and an appropriate scalar. It is well-known that the smaller the mesh size, the better the result is obtained. However, the small mesh size results in a high computational cost. When mesh size is reduced to a certain value, the convergence of solution is expected. In this study, the basic meshing number of 8 elements is sufficient to ensure the convergence of the FE solution.

From the FE solution of the magnetic circuit, the induced MRF rheological properties in the ducts such as the yield stress ( $\tau_{ye}$ ,  $\tau_{yj}$ ,  $\tau_{ya}$ ) and the post yield viscosity ( $\mu_e$ ,  $\mu_{ej}$ ,  $\mu_a$ ) are calculated by Equation (11) via the average induced magnetic density and its initial rheological parameters. From the obtained values of all abovementioned parameters, the on-state of each MRB can be then estimated by Equations (8, 9). From geometric dimensions, the off-state torque can be calculated by Equation



(10) while the mass and the power consumption of the MRBs can be determined from Equations (13, 14), respectively. It is noted that these performance parameters are updated in each optimization loop. In this research, the optimization procedure is conducted by using the first order optimization method with the gradient decent algorithm. The procedures to achieve optimal design parameters of the MRBs using the first order method of ANSYS optimization tool is shown in **Figure 3**. Starting with initial value of design variables, by executing the ANSYS log-file, performance characteristics of the MRBs at the first iteration are calculated. The ANSYS optimization tool then transforms the constrained optimization problem to an unconstrained one via penalty functions. For the initial iteration, the search direction of DVs is assumed to be the negative of the gradient of the unconstrained objective function. In the subsequent iterations, the direction vectors are calculated according to Polak-Ribiere recursion formula. A detailed description of this algorithm integrated with ANSYS software is shown in previous research (Nguyen et al., 2007).

## RESULTS AND DISCUSSIONS

In this section, the optimal results of the MRBs are obtained with different types of MRF and discussions on the effects of MRF types on performance parameters of the MRBs are presented. **Table 1** shows the materials selections for components of MRBs. As shown in the table, the commercial silicon steel is used for magnetic components of the MRB such as the housing and the disc, the bobbin is made of non-magnetic steel, the coil is made from copper wire sized as 24-gage (diameter = 0.511 mm) whose maximum working current is around 3 A and during the optimization process an applied current of 2.5 A is used. Three types of commercial MR fluid made by Lord Corporation: MRF-122-2ED (low yield stress), MRF-132-DG (medium yield stress) and MRF-140 CG (high yield stress) are considered. Parameters of the field dependent Bingham rheological model of the MRF are determined from experimental results using curve fitting method as shown in **Figure 5**. In this research work, a least square

**TABLE 1** | Magnetic property of the brake components.

Brake components	Material	Relative permeability	Saturation flux density
Disc, Housing	Silicon Steel	B-H Curve (Figure 4A)	1.55 Tesla
Coil	Copper (24-gage)	1	X
MR Fluid	MRF-122-2ED	B-H curve (Figure 4B)	1.5 Tesla
	MRF-132-DG		1.65 Tesla
	MRF-140-CG		1.75 Tesla
Bobbin, Shaft	Non-magnetic Steel	1	X

curve fitting method is used, and the results are presented in **Table 2** (Nguyen and Choi, 2010).

In the optimization, the design variables are significant geometric dimensions of the MRBs such as the coil height  $h_c$ , the coil width  $w_c$ , the inner radius of the disc  $R_i$ , the outer radius of the disc  $R_d$ , the disc thickness  $t_d$ , outer radius of the brake  $R$ , the housing thickness  $t_h$ , the inner radius of the coils in case of the side-coil MRBs  $R_c$ , and the gap size of the MRF ducts are also considered as design variables. It is noted that the shaft radius is set by  $R_s = 8$  mm in the optimization.

**Figures 6–11** show optimal solutions of the MRB when the mass is considered as the objective function at different values of the constrained braking torque, ranging from 5 to 100 Nm. It is noted that this case is equivalent to the case when the weighting coefficients in the objective function in Equation (12) are chosen at  $\alpha_m = 1.0$ ,  $\alpha_p = \alpha_{T_o} = 0$ . The smaller value of the MRF gap size in the higher braking torque can be archived and the smaller mass of the MRB is. Therefore, during the optimization process, the MRF gap size is not considered as a design variable and fixed at a certain value. In these figures, three typical values of the gap size, which are 0.6, 0.8, and 1.0 mm, are considered. In **Figures 6, 7**, the gap size is set by 0.6 mm. It is observed from the figure that when we consider only the mass of the MRBs in the optimization, MRBs employing the highest yield stress MRF have the smallest mass and power consumption at all values of the constrained braking torque. However, the off-state torque of the MRB with highest yield stress is significantly greater than the others. Therefore, if the brake normally works in off-state condition, this issue should be taken into account. It also observed from the figures that among the three MRFs, the medium yield stress MRF (MRF 132-DG) is the most compromised of the three mentioned performance parameters, the mass, the power consumption and the off-state force. The off-state torque in the case of MRB with MRF 132-DG is even smaller than the MRB with low yield stress MRF (MRF-122-2ED). The reason is that the MRB employing MRF-122-2ED has a larger disc radius to produce enough braking torque, which also results in corresponding higher off-state torque. By comparison at different values of the MRF gap size, it is observed that the smaller the gap size, the smaller the mass of the MRBs that can be archived, and the lower the power consumed by the coils. However, the off-state torque of the MRBs increases as the MRF gap size decreases and this should be taken into

account especially when the MRBs work continuously such as in automotive application.

**Figures 12, 13** show optimal solutions of the MRBs, when the weighting coefficients of the objective function in Equation (12) are chosen at  $\alpha_m = \alpha_p = \alpha_{T_o} = 1/3$ , at different values of the constrained braking torque ranging from 5 to 100 Nm. This means that the importance of the three performance parameters (the mass, the power consumption and the off-state torque) are assumed equal. It is noted that in this case the gap size of MRF is also considered as a design variable, ranging from 0.6 to 1.0 mm. The results show that by considering all three issues (multi-objective optimization) in the optimization, a compromised optimal result can be archived. By comparing **Figures 12, 13** with the previous figures (**Figures 6–11**), it is observed that in case of multi-objective optimization, the mass of the MRBs is a bit greater than that in case of mass optimization; however the power consumption and off-state torque are significantly smaller. Again, the same comments can be obtained by considering different types of MRF from **Figures 12, 13**, which mean that the medium yield stress MRF (MRF 132-DG) is the most compromised among the three considered MRFs. The gap size of MRBs at the optimum is equal to its lower limit, which is 0.6 mm.

**Figures 14, 15** show optimal solutions of the MRBs, when the weighting coefficients of the objective function in Equation (12) are chosen at  $\alpha_m = \alpha_p = 0.5$  and  $\alpha_{T_o} = 0$ , which means that the importance of the mass and the power consumption are assumed equal while the off-state torque is not considered. The results show that the mass of the MRBs is a bit smaller than that in **Figures 12, 13** and the power consumption of the MRBs is significantly reduced, especially for the MRBs employing MRF 132-DG, while the off-state of the MRBs are slightly increased. From **Figures 14, 15**, again it is observed that the medium yield stress MRF (MRF 132-DG) is the most compromised among the three considered MRFs. The gap size of MRBs at the optimum is equal to its lower limit in this case, as well.

**Figures 16, 17** show optimal solutions of the MRBs, when the weighting coefficients of the objective function in Equation (12) are chosen at  $\alpha_m = 0.5$ ,  $\alpha_p = 0.0$  and  $\alpha_{T_o} = 0.5$ , which means that the importance of the mass and the off-state torque are assumed equal while the power consumption is not considered. The results show that the mass of the MRBs is almost the same as that in **Figures 14, 15**. This is because the weighting coefficient is the same in both cases. However, the power consumption is much higher than that of the previous case, although the off-state torque is smaller. Similar to **Figures 14, 15**, the medium yield stress MRF (MRF 132-DG) is the most compromised among the three considered MRFs. Again, the gap size of MRBs at the optimum is equal to its lower limit.

**Figures 18, 19** show optimal solutions of the MRBs, when the weighting coefficients of the objective function in Equation (12) are chosen at  $\alpha_m = 0.75$ ,  $\alpha_p = 0.0$  (power consumption is not considered) and  $\alpha_{T_o} = 0.25$ . By comparing with **Figures 16, 17** it is observed that the mass of the MRBs is a bit smaller in this case while the off-state torque is a bit higher. However, the power consumption is much smaller than the previous case. Therefore, if the optimization considers only mass and off-state torque, it is recommended that the weighting coefficients should be set by

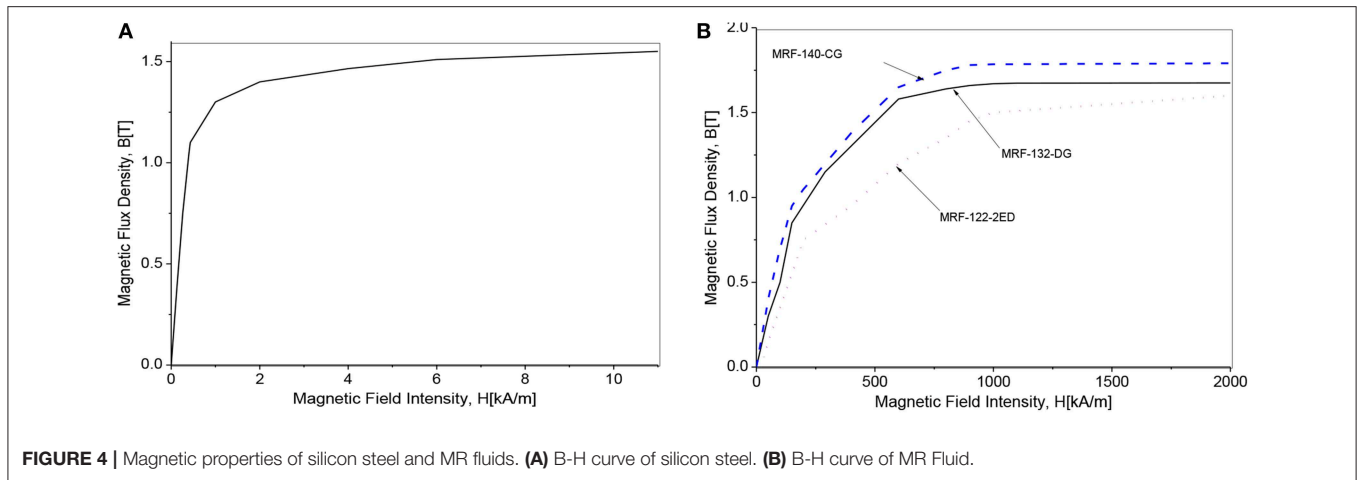


**FIGURE 4** | Magnetic properties of silicon steel and MR fluids. **(A)** B-H curve of silicon steel. **(B)** B-H curve of MR Fluid.

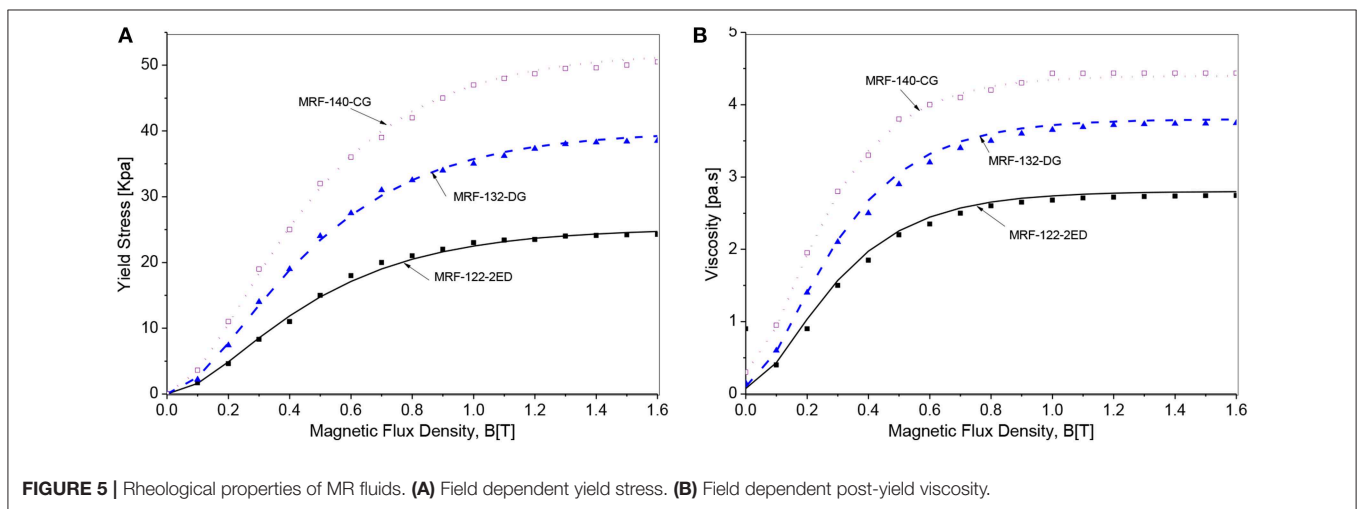


**FIGURE 5** | Rheological properties of MR fluids. **(A)** Field dependent yield stress. **(B)** Field dependent post-yield viscosity.

**TABLE 2** | Rheological properties of MR fluids.

MR fluid	Bingham model
MRF-122-2ED	$\mu_0 = 0.075pa \bullet s; \mu_\infty = 2.8pa \bullet s; \alpha_{S\mu} = 4.5T^{-1}$ $\tau_{y0} = 12pa; \tau_{y\infty} = 25200pa; \alpha_{st\gamma} = 2.9T^{-1}$
MRF-132DG	$\mu_0 = 0.1pa \bullet s; \mu_\infty = 3.8pa \bullet s; \alpha_{S\mu} = 4.5T^{-1}$ $\tau_{y0} = 15pa; \tau_{y\infty} = 40000pa; \alpha_{st\gamma} = 2.9T^{-1}$
MRF-140CG	$\mu_0 = 0.29pa \bullet s; \mu_\infty = 4.4pa \bullet s; \alpha_{S\mu} = 5T^{-1}$ $\tau_{y0} = 25pa; \tau_{y\infty} = 52000pa; \alpha_{st\gamma} = 3T^{-1}$

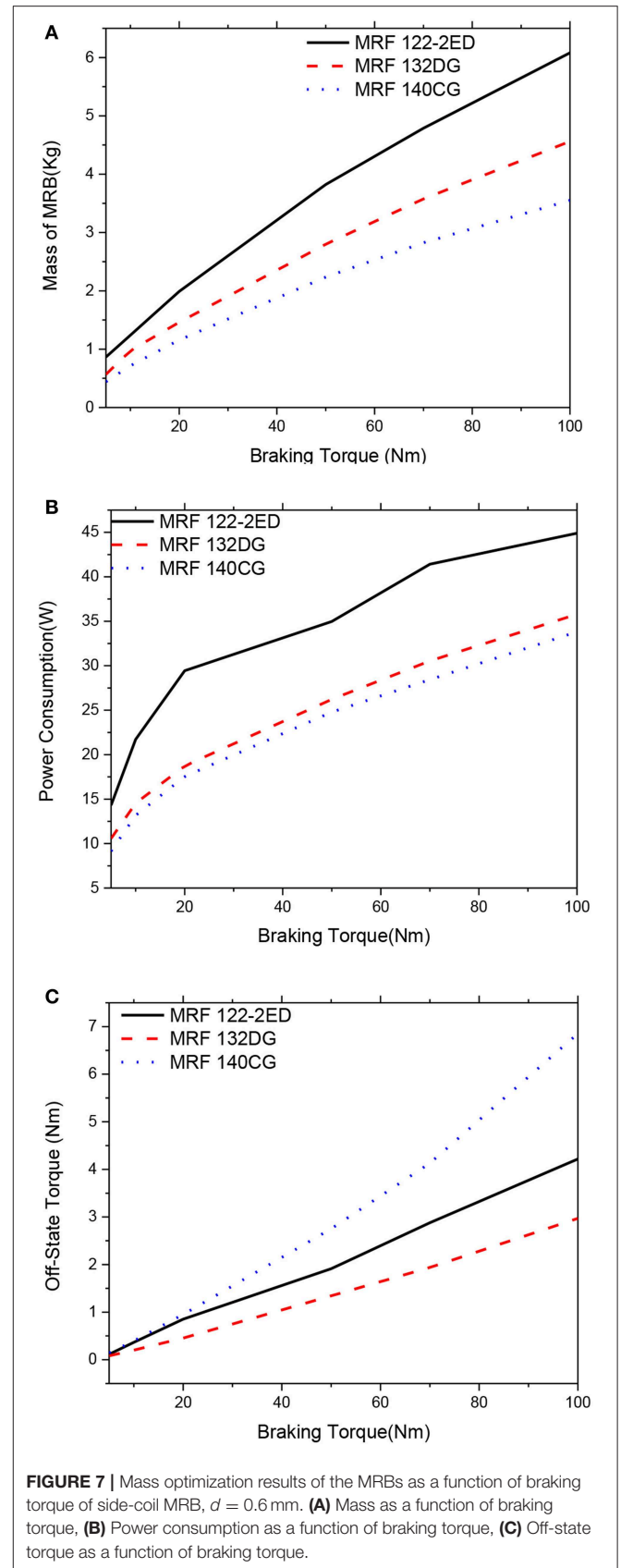
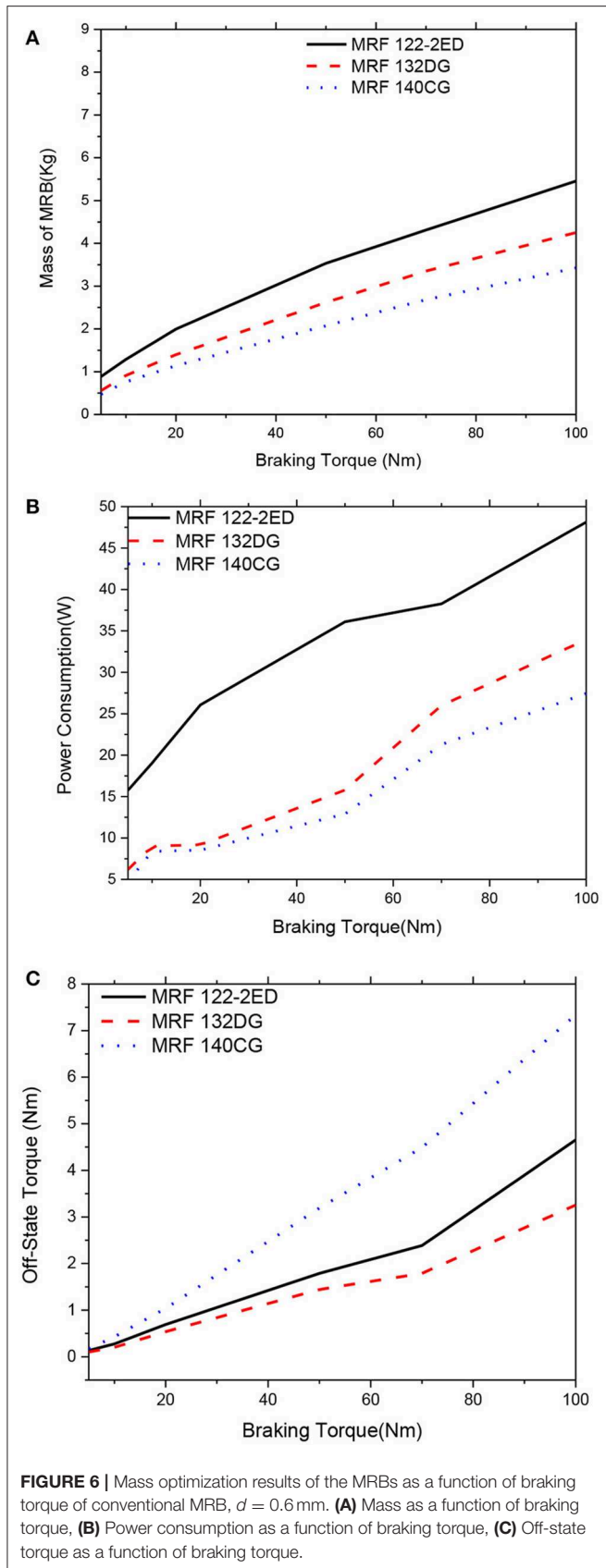
$\alpha_m = 0.75$ ,  $\alpha_p = 0.0$ , and  $\alpha_{T_o} = 0.25$  rather than  $\alpha_m = 0.5$ ,  $\alpha_p = 0.0$ , and  $\alpha_{T_o} = 0.5$ . The gap size of MRBs at the optimum is also equal to its lower limit.

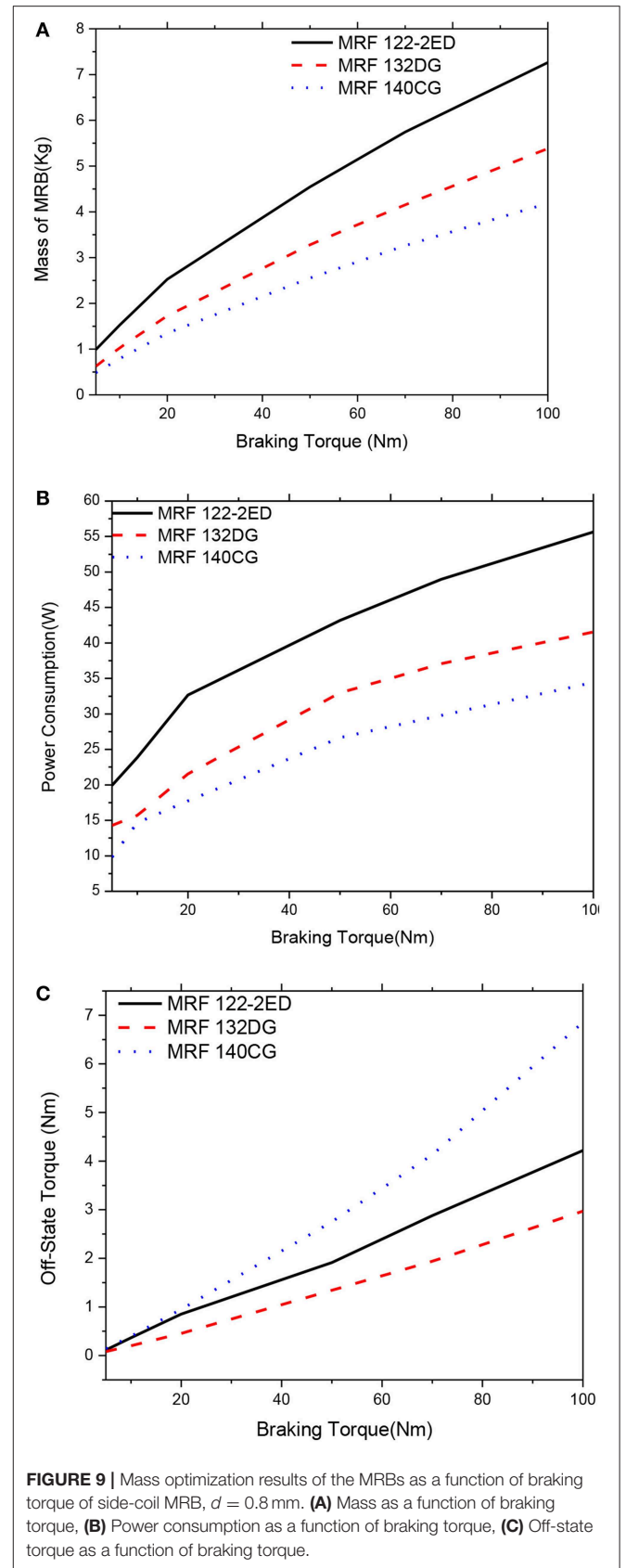
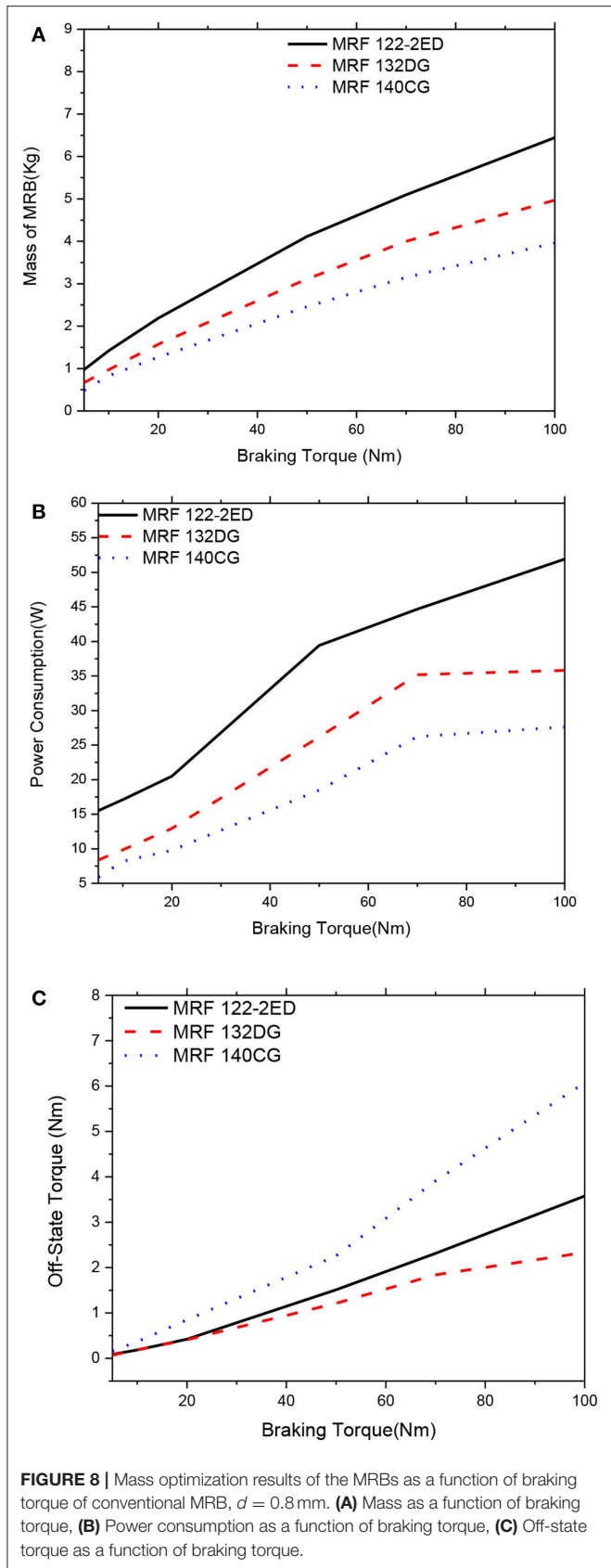
From all of the above, it can be summarized as the following:

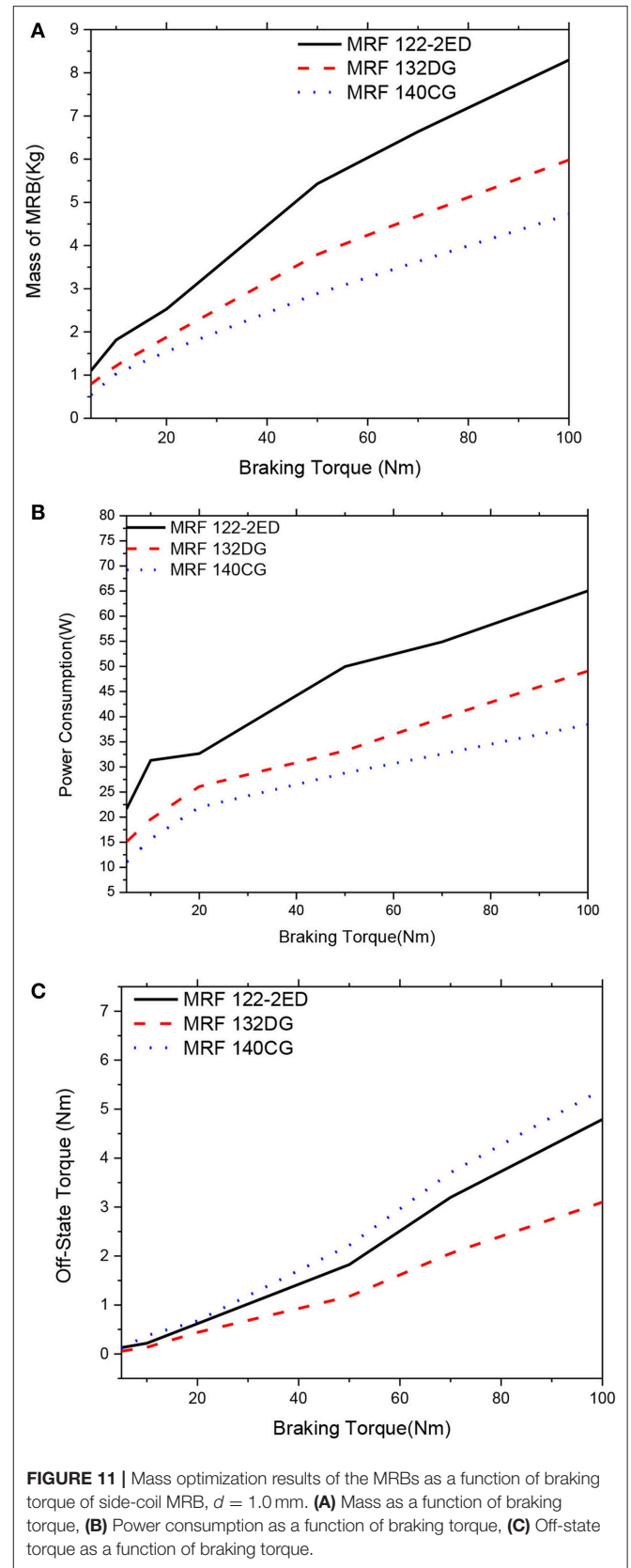
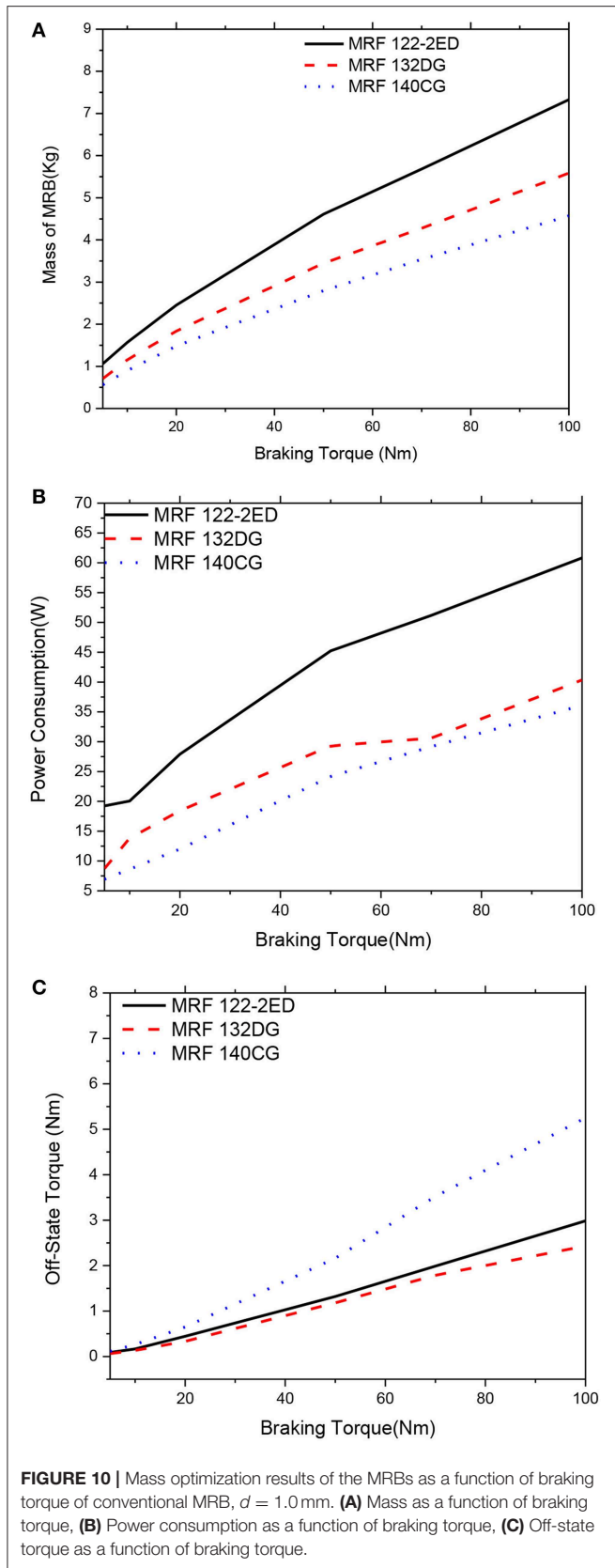
- An objective function which is a linear combination of the mass, the power consumption and the off-state torque can be used for multi-objective optimization of MRBs. By assigning different values of weighting coefficients in the objective function, different optimal solutions can be archived. To get the most compromised of the three objective performances,

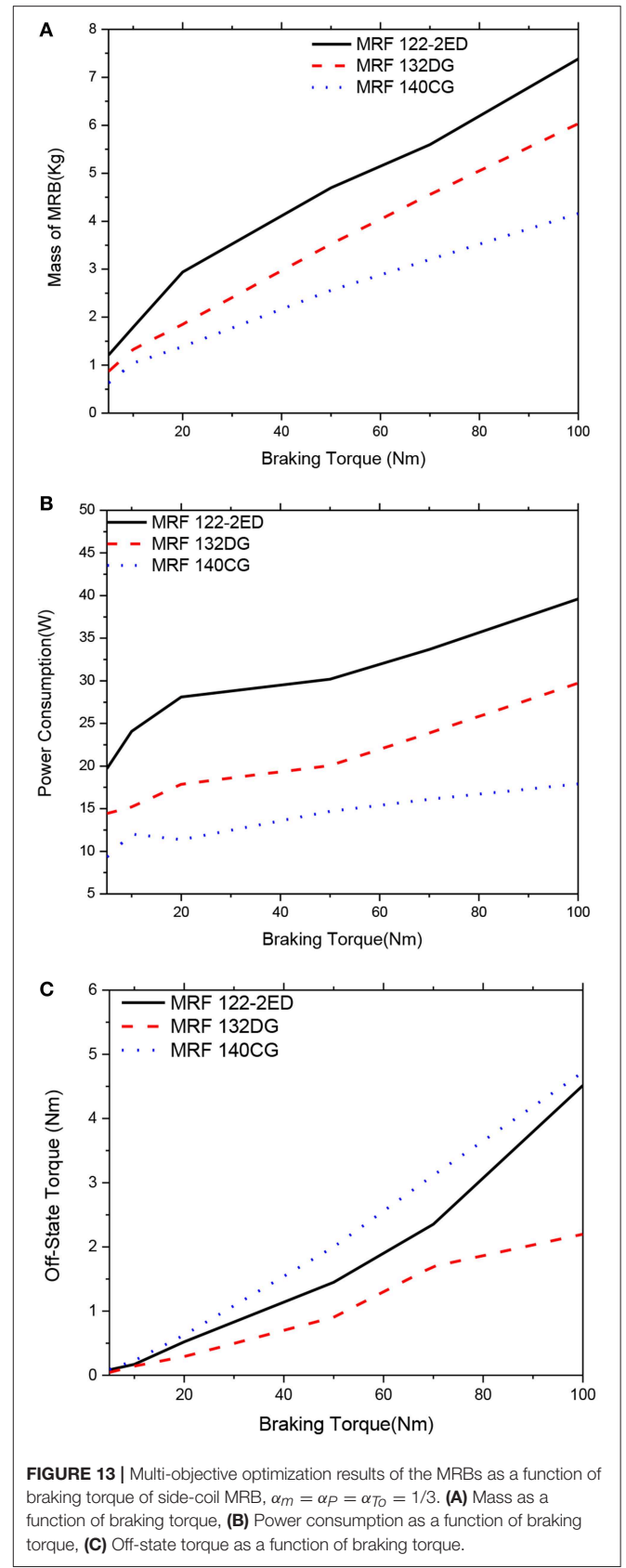
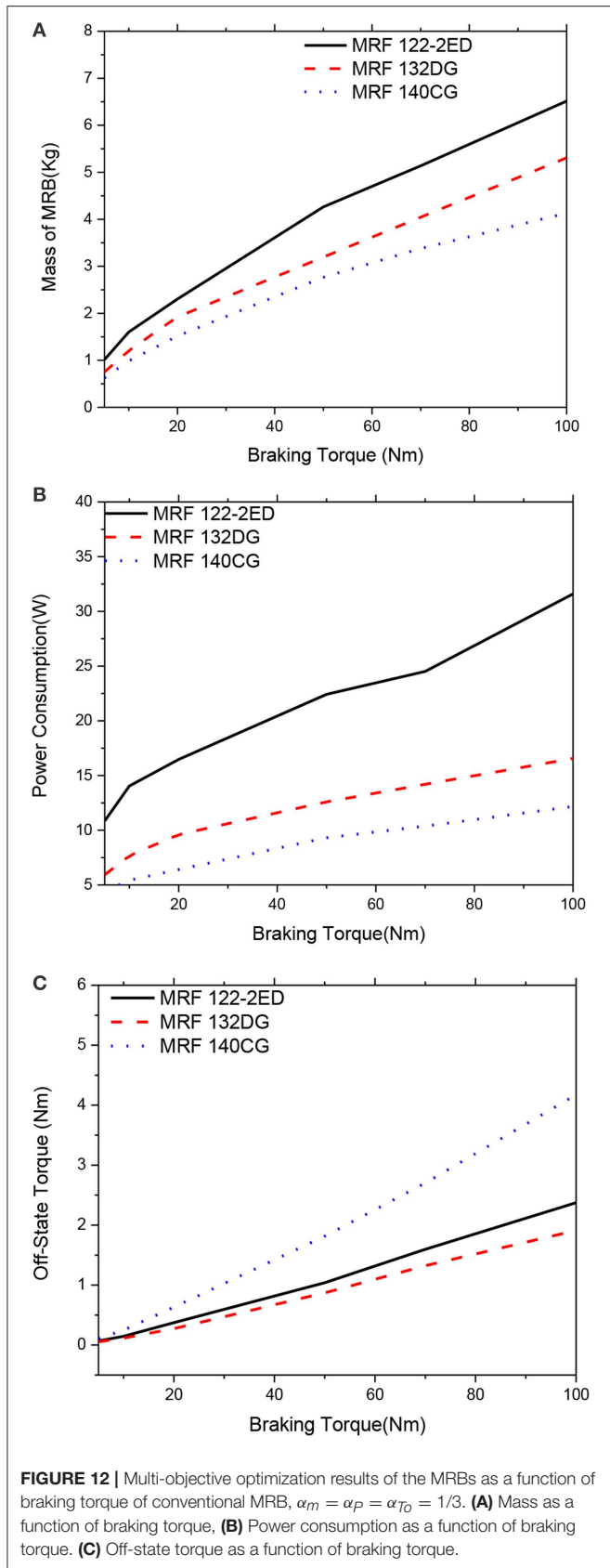
a real multiobjective algorithm to get Pareto front solution should be implemented.

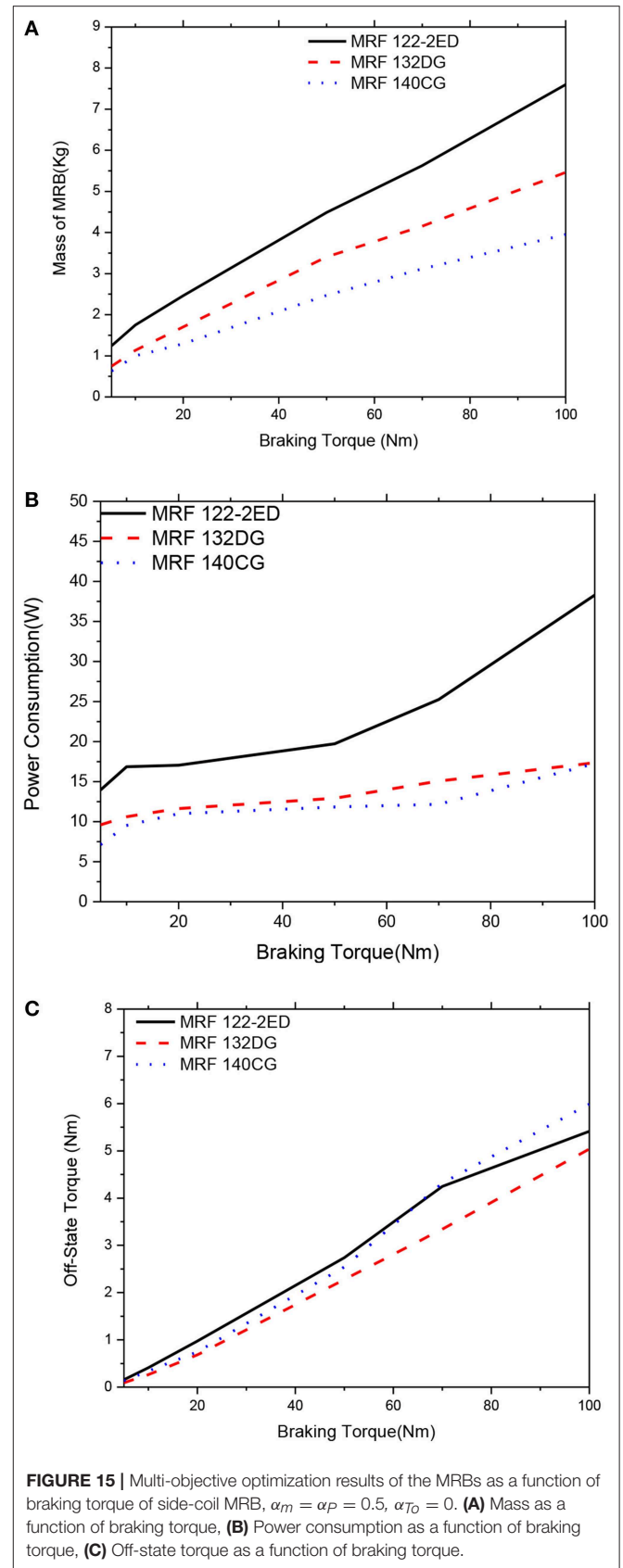
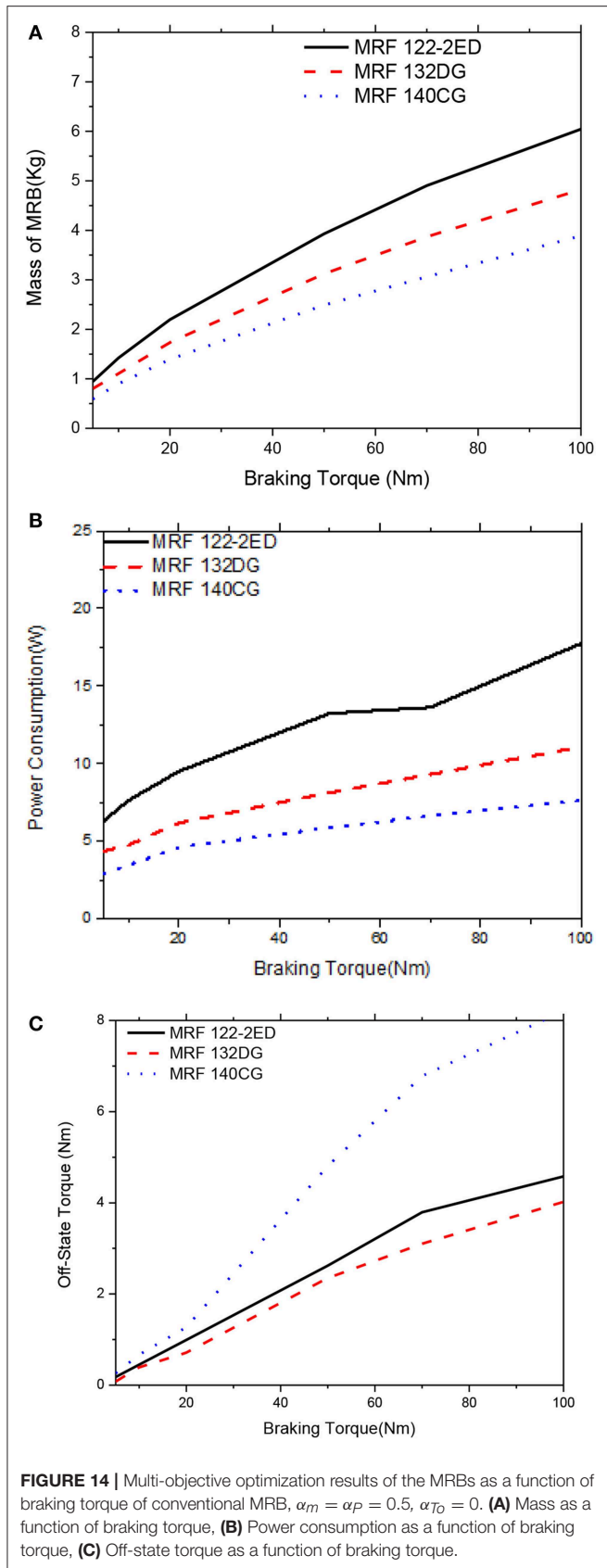
- In the optimization, it is not necessary to consider the gap size of the MRF as a design variable. In most cases, the gap size of MRF should be selected to be as small as possible considering manufacturing convenience.
- At the optimum, the MRBs employing the highest yield stress MRF (MRF-140CG) always have the smallest mass and power consumption, however, the off-state torque is significantly larger than the others. Therefore, in case the off-state torque is not important for the brake, highest yield stress MRF (MRF-140CG) is recommended for MRB application.
- At the optimum, the MRBs employing the lowest yield stress MRF (MRF-122-2ED) have the largest mass and power consumption, while the off-state torque is larger than that in case of medium yield stress MRF (MRF-132-DG). Therefore, lowest yield stress MRF (MRF-122-2ED) is not recommended for MRB application
- At the optimum, the MRBs employing the medium yield stress MRF (MRF-132DG) have the compromised performance when the off-state torque is considered in the objective

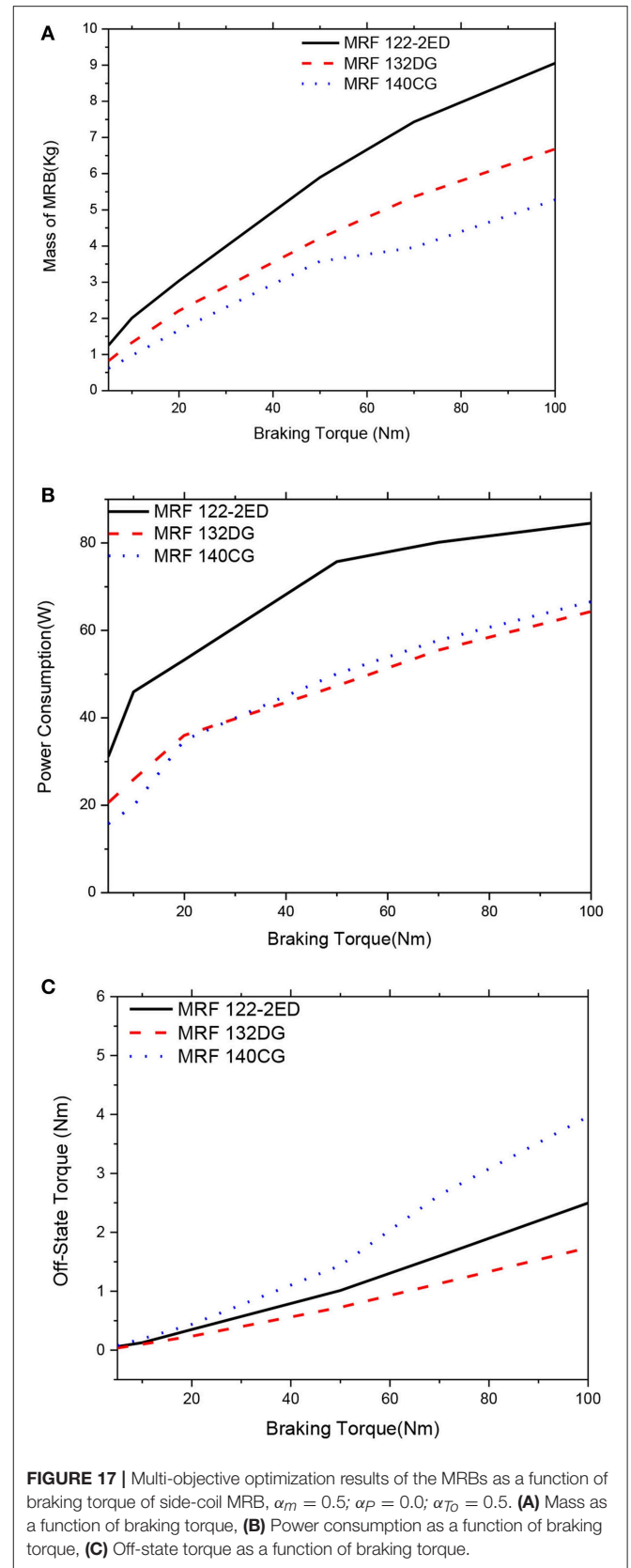
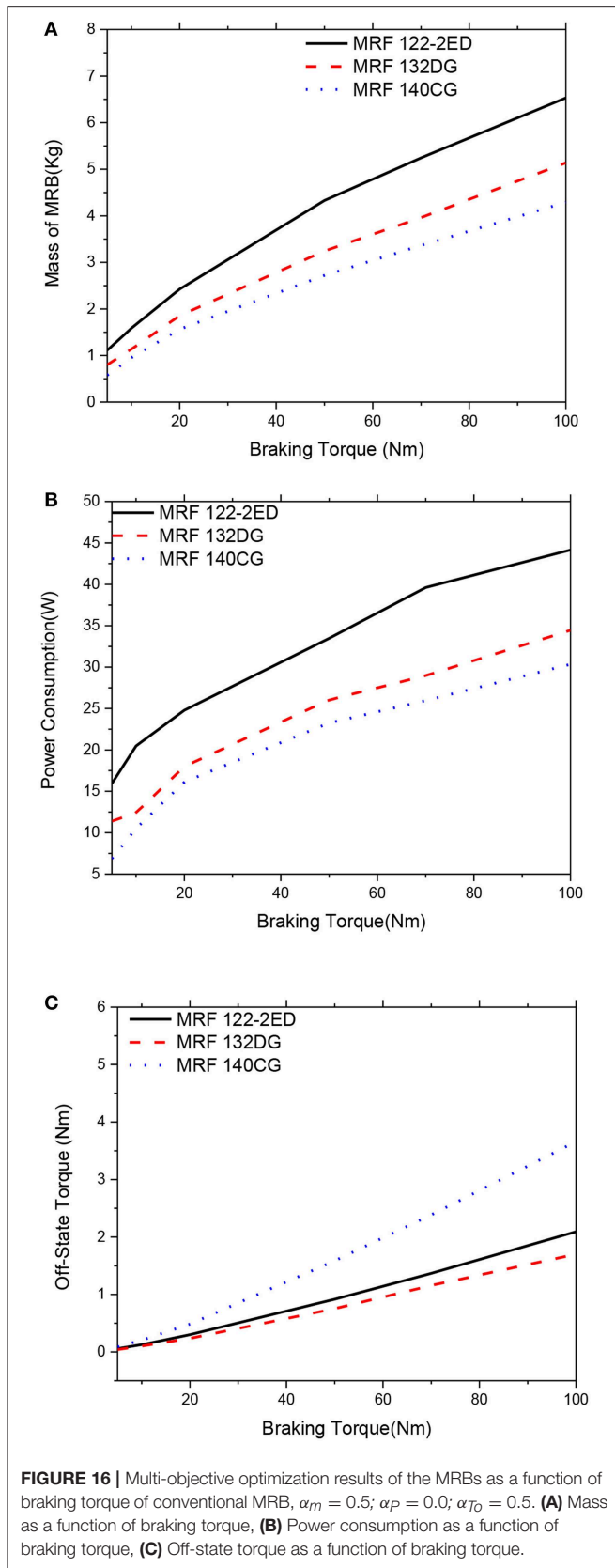


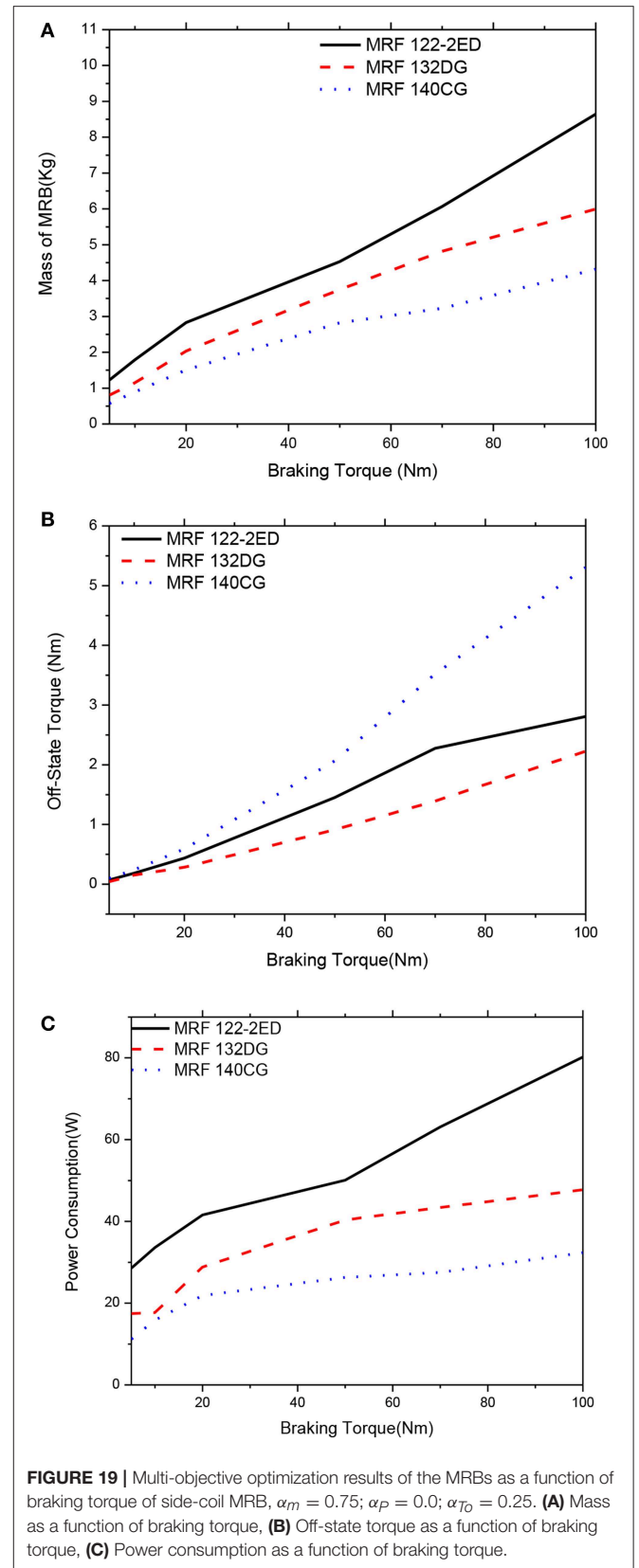
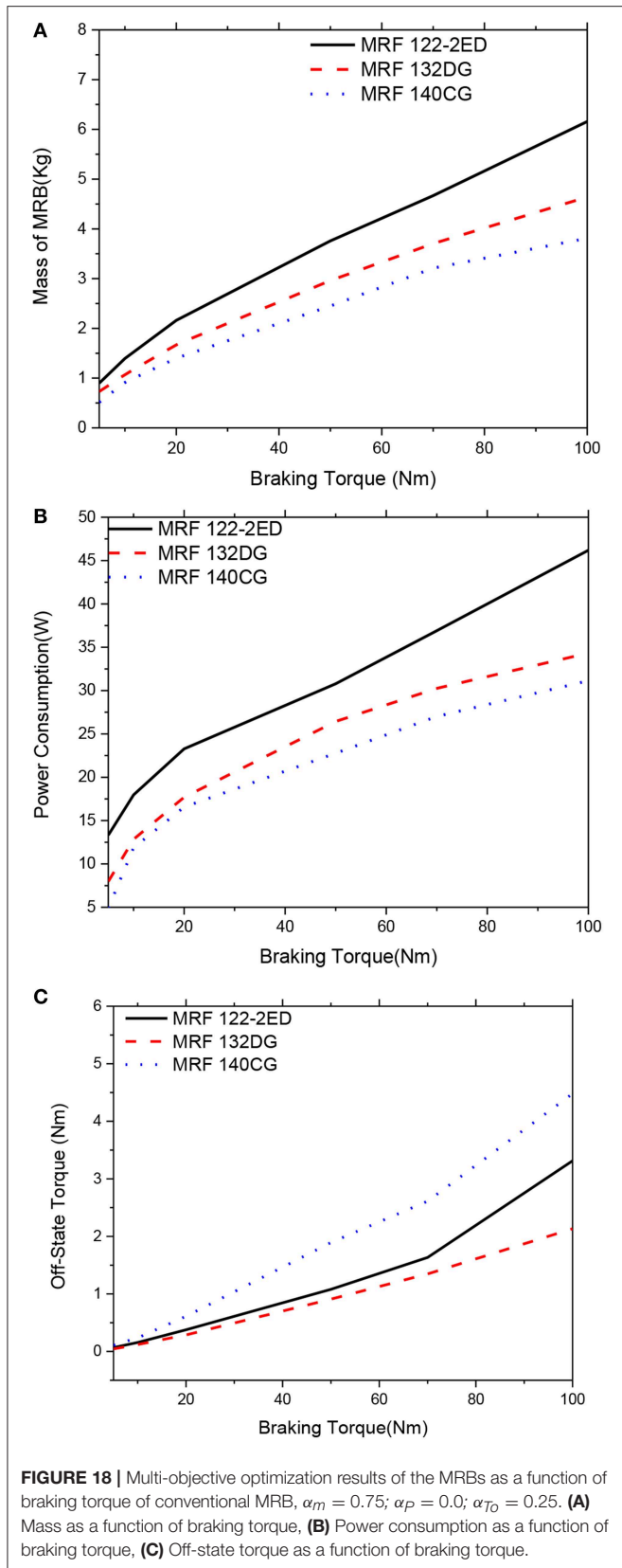












function. Therefore, in most cases, the medium yield stress MRF (MRF-132DG) is the recommended MRB application.

## CONCLUSIONS

In this research work, a multi-objective function considering mass, power consumption and off-state torque was proposed for the optimal design of MRBs. Based on the proposed optimization, material characterization of MRFs on the performance of the MRBs were investigated. Three different types of popular commercial MRFs: MRF-122-2ED (low yield stress), MRF-132-DG (medium yield stress) and MRF-140CG (high yield stress) and two typical disc type MRBs: the conventional and the side-coil MRB were considered. The simulation results show that, at the optimum, the MRBs employing MRF-140CG always have the smallest mass and power consumption, however, the off-state torque is significantly larger than the others. Therefore, in case the off-state torque is not important for the brake, MRF-140CG is recommended for MRB application. It is also found that performance of the MRBs employing MRF-122-2ED was always worse than the MRF132-DG. Therefore, the lowest

yield stress MRF (MRF-122-2ED) is not recommended for MRB application. Among the three considered MRFs, MRF-132DG had the best compromised performance. Especially, in the case of  $\alpha_m = 0.5$ ;  $\alpha_P = 0.0$ ;  $\alpha_{T_0} = 0.5$ . Therefore, in the design of MRBs that need to compromise different conflict benefit performance characteristics, MRF-132DG is the recommended MRB application. Finally, it is found that, in the optimization, it is not necessary to consider the gap size of the MRF as a design variable. In most cases, the gap size of MRF should be selected as small as possible considering manufacturing convenience.

## AUTHOR CONTRIBUTIONS

All authors listed have made a substantial, direct and intellectual contribution to the work, and approved it for publication.

## ACKNOWLEDGMENTS

This research is funded by Vietnam National Foundation for Science and Technology Development (NAFOSTED) under grant number 107.01-2016.32.

## REFERENCES

- An, J., and Kwon, D.-S. (2003). Modeling of a magnetorheological actuator including magnetic hysteresis. *J. Intellig. Mater. Syst. Struct.* 14, 541–550. doi: 10.1177/104538903036506
- Avraam, M., Horodincă, M., Letier, P., and Preumont, A. (2008). “Portable smart wrist rehabilitation device driven by rotational MR-fluid Brake actuator for telemedicine applications,” in *IEEE/RSJ International Conference on Intelligent Robots and Systems*, (Nice).
- Avraam, M., Horodincă, M., Romanescu, I., and Preumont, A. (2010). Computer controlled rotational MR-brake for wrist rehabilitation device. *J. Intellig. Mater. Syst. Struct.* 21, 1–15. doi: 10.1177/1045389X10362274
- Huang, J., Zhang, J. Q., Yang, Y., and Wei, Y. Q. (2002). Analysis and design of a cylindrical magneto-rheological fluid brake. *J. Mater. Proc. Technol.* 129, 559–562. doi: 10.1016/S0924-0136(02)00634-9
- Imaduddin, F., Mazlan, S. A., and Zamzuri, H. (2013). A design and modeling review of rotary magnetorheological damper. *Mater. Design.* 51, 575–591. doi: 10.1016/j.matdes.2013.04.042
- Liu, B., Li, W. H., Kosasih, P. B., and Zhang, X. Z. (2006). Development of an MR-brake-based haptic device. *Smart Mater. Struct.* 15, 1960–1966. doi: 10.1088/0964-1726/15/6/052
- Mousavi, S. H., and Sayyaadi, H. (2018). Optimization and testing of a new prototype hybrid MR brake with arc form surface as a prosthetic knee. *IEEE ASME Trans. Mechatron.* 23, 1204–1214. doi: 10.1109/TMECH.2018.2820065
- Nguyen, Q. H., and Choi, S. B. (2010). Optimal design of an automotive magnetorheological brake considering geometric dimensions and zero-field friction heat. *Smart Mater. Struct.* 19:115024. doi: 10.1088/0964-1726/19/11/115024
- Nguyen, Q. H., and Choi, S. B. (2011). Selection of magnetorheological brake types via optimal design considering maximum torque and constrained volume. *Smart Mater. Struct.* 21:15012. doi: 10.1088/0964-1726/21/1/015012
- Nguyen, Q. H., and Choi, S. B. (2012). Optimal design of a novel hybrid MR brake for motorcycles considering axial and radial magnetic flux. *Smart Mater. Struct.* 21:55003. doi: 10.1088/0964-1726/21/5/055003
- Nguyen, Q. H., Han, Y. M., Choi, S. B., and Wereley N. M. (2007). Geometry optimization of MR valves constrained in a specific volume using the finite element method. *Smart Mater. Struct.* 16, 2242–2252. doi: 10.1088/0964-1726/16/6/027
- Nguyen, Q. H., Lang, V. T., Nguyen, N. D., and Choi S. B. (2014a). Geometric optimal design of a magneto-rheological brake considering different shapes for the brake envelope. *Smart Mater. Struct.* 23:15020. doi: 10.1088/0964-1726/23/1/015020
- Nguyen, Q. H., Nguyen, N. D., and Choi, S. B. (2014b). “Design and evaluation of a novel configuration of MR brake with coils placed on the side housings,” in *Proceedings of the SPIE*. doi: 10.1117/12.2044561
- Nguyen, Q. H., Nguyen, N. D., and Choi, S. B. (2015). Design and evaluation of a novel MR brake with coils placed on side housings. *Smart Mater. Struct.* 24:90590I. doi: 10.1088/0964-1726/24/4/047001
- Park, E. J., Stoikov, D., Falcao da Luz, L., and Suleman A. (2006). A performance evaluation of an automotive magnetorheological brake design with a sliding mode controller. *Mechatronics* 16, 405–416. doi: 10.1016/j.mechatronics.2006.03.004
- Smith, A. L., Ulicny, J. C., and Kennedy, L. C. (2007). Magnetorheological fluid fan drive for trucks. *J. Intellig. Mater. Syst. Struct.* 18, 1131–1136. doi: 10.1177/1045389X07083136
- Zubieta, M., Eceolaza, S., Elejabarrieta, M. J., and Bou-Ali, M. M. (2009). Magnetorheological fluids: characterization and modeling of magnetization. *Smart Mater. Struct.* 18:95019. doi: 10.1088/0964-1726/18/9/095019

**Conflict of Interest Statement:** The authors declare that the research was conducted in the absence of any commercial or financial relationships that could be construed as a potential conflict of interest.

Copyright © 2019 Quoc, Tuan, Hiep, Quoc and Choi. This is an open-access article distributed under the terms of the Creative Commons Attribution License (CC BY). The use, distribution or reproduction in other forums is permitted, provided the original author(s) and the copyright owner(s) are credited and that the original publication in this journal is cited, in accordance with accepted academic practice. No use, distribution or reproduction is permitted which does not comply with these terms.